Tetrahedron: *Asymmetry* 19 (2008) 2140–2148

Contents lists available at ScienceDirect

Tetrahedron: *Asymmetry*

journal homepage: www.elsevier.com/locate/tetasy

# A DFT study of 1,3-dipolar cycloadditions of cyclic nitrones to unsaturated lactones. Part II

Sebastian Stecko [a], Konrad Paśniczek [a], Carine Michel [b], Anne Milet [b], Serge Perez [c], Marek Chmielewski [a,*]

[a] *Institute of Organic Chemistry of the Polish Academy of Sciences, Kasprzaka 44/52, 01-224 Warsaw, Poland*
[b] *Département de Chimie Moléculaire, Université Joseph Fourier, BP53, 38041 Grenoble, France*
[c] *Centre de Recherches sur les Macromolécules Végétales, CNRS, BP53, 38041 Grenoble, France*

ARTICLE INFO

*Article history:*
Received 17 July 2008
Accepted 4 September 2008
Available online 10 October 2008

ABSTRACT

The 1,3-dipolar cycloadditions of cyclic nitrones to five-membered unsaturated lactones are studied. Special attention was focused on a single and double asymmetric induction when one or both components were chiral. The energies of the cycloaddition reactions are investigated through application of molecular orbital calculations at the B3LYP/6-31+G(d) theory level. A study of the different reactants' approaches and their conformational aspects revealed the stereochemical preferences of these reactions. The results of these calculations correspond well with the previously reported experimental data.



## 1. Introduction

The 1,3-dipolar cycloadditions (1,3-DCs) between nitrones and alkenes are a very useful tool for the construction of isoxazolidines. The latter, after cleavage of the nitrogen–oxygen bond, can be transformed into β-aminoalcohols.[1] Owing to these attractive possibilities, such reactions are frequently used in the target-oriented synthesis of nitrogen-containing products.[2]

As part of our research on the application of 1,3-DC reactions in synthesis of polyhydroxy-alkaloids,[3] we have recently reported studies on the reactions of five-membered cyclic nitrones with γ- and δ-lactones.[4–6] In the case of δ-lactones, the reactions usually showed high diastereoselectivity and the exclusive formation of *exo*-adducts.[4] In marked contrast to δ-lactones, the five-membered lactones reacted with a lower diastereoselectivity and led to the mixtures of products. This is a consequence of formation of *endo*-products and the reversibility of the reaction.[5,6] Such a course of reaction has never been observed for δ-lactones.[4]

Recently, we have presented a DFT study on the 1,3-DCs of nitrone **N1** to the lactones **L1**/**L2** and vinyl ethers **E1**/**E2** (Chart 1).[8] The calculated predictions were in good agreement with the experimental results.[7,9,10] For lactones, the *meta*-regioselectivity has been predicted, whereas for ethers, which have an opposite electronic character, the *ortho*-regioselectivity was usually observed. In all cases, the *exo*-adducts were found to have a lower energy transition state than the *endo* ones. It has also been pointed out that the high diastereoselectivity of the 1,3-DCs with six-membered dipolarophiles (which is manifested by the exclusive formation of *exo*-adducts) is the result of a steric repulsion in their *endo* transition state (TS).[8]

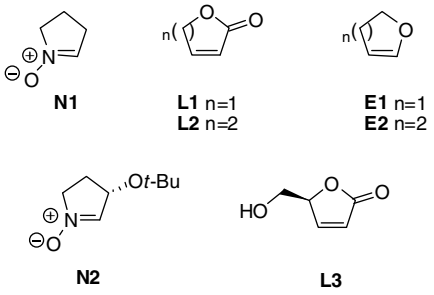


**Chart 1.**

The DFT calculations and experimental observations[8] prompted us to conduct further studies on 1,3-DCs of cyclic nitrones to the cyclic dipolarophiles, particularly to analyze the cases of chiral reactants, the lactone or nitrone, or both. Herein, we report studies on the reactions of nitrones **N1** and **N2** with 2-(5*H*)-furanones: **L1**, **L3**, and *ent*-**L3**.

## 2. Computational methods

All calculations were carried out using the GAUSSIAN 03 suite of software.[11] The geometry optimization of critical points (reactants, transition structures, and products) was carried out using DFT method at the B3LYP/6-31+G(d) level theory.[12] The stationary points were characterized by the frequency calculations to verify that both the minima and the transition structures (TSs) have zero

* Corresponding author. Tel./fax: +48 22 632 66 81.
*E-mail address:* chmiel@icho.edu.pl (M. Chmielewski).

0957-4166/$ - see front matter © 2008 Elsevier Ltd. All rights reserved.
doi:10.1016/j.tetasy.2008.09.003

and one imaginary frequency, respectively. The optimizations were carried out using the Berny analytical gradient optimization method.[13] The electronic structures of the critical points were studied by the natural bond orbital (NBO) method.[14] The intrinsic reaction coordinates (IRC)[15] were also calculated to analyze the mechanism in detail for all the transition structures. The molecular modeling was carried out using HYPERCHEM 7.5 software (HyperCube, Inc.).

According to the experimental observations, for each presented reaction only one regioisomeric approach of reactants[8] was investigated, while both the *exo* and *endo* approaches of reactants were analyzed.

## 3. Results and discussion

### 3.1. Conformation analysis of tricyclic fused system

The conformational search using the MM+ force field for the two simplest unsubstituted adducts **P1** (*exo*) and **P2** (*endo*) (Chart 2) showed the presence of several conformers (Fig. 1). The extended search (scanning range) also allowed us to find the energy of invertomers **P1*c4*** and **P2*c3*** (Fig. 1, type III). Their large values of relative energy suggest a high barrier of inversion of configuration at the nitrogen atom. This result correlates well with the fact that stereoisomers related to inversion at the nitrogen atom of the 5–5–5 fused tricyclic systems have never been observed by us,[5,6] or by Font and de March.[7b] On the other hand, both invertomers can be easily observed for systems having six-membered C-ring derived from the nitrone and the five-, six-, or seven-membered lactone ring.[1,3e,7a,c] All conformers of **P1** and **P2** are depicted in Figure 1.

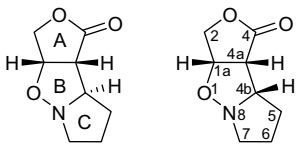


**P1** **P2**

**Chart 2.**

Two types of conformers were found for **P1** adduct (Fig. 1, type I and II). The most significant difference between these conformers is the location of the oxygen atom of isoxazolidine in relation to the $C_{1a}$–$C_{4a}$–$C_{4b}$–$N_8$ plane, Figure 1. The most stable **P1** conformer (**P1*c1***) has an almost flat A-ring with a coplanar arrangement of $O_1$, $C_{1a}$, $C_{4a}$ and $C_{4b}$ atoms of B-ring (only the nitrogen atom is located out-of-plane). For the two high-energy conformers **P2*c2*** and **P1*c3***, the lactone ring A is twisted. In the latter case, atoms $C_{1a}$, $C_{4a}$, $C_{4b}$, and $N_8$ of the B-ring are almost coplanar while the $O_1$ atom is located out-of-plane. The geometries of **P1*c2*** and **P1*c3*** are very close, differing mostly by the conformation of the C rings.

In contrast to **P1**, the **P2** cycloadduct has only one set of conformers (type II). The **P2*c1*** and **P2*c2*** differ by the location of the $N_8$ atom in relation to the $O_1$–$C_{1a}$–$C_{4a}$–$C_{4b}$ plane, which influences the C-ring conformation. In further studies, for each investigated reaction, the two most stable conformers of the product were taken into consideration. Such geometry of the reactants' approach gave a better idea of the cycloaddition, and we were able to determine that the type II structures correspond better to the related transition state than the type I structures.

### 3.2. The 1,3-DC reaction of nitrone N2 and lactone L 1—single asymmetric induction system

The cycloaddition of the nitrone **N2** to the unsubstituted lactone **L1** theoretically may afford four products: two *exo*- (**P3**, **P4**) and two *endo*-adducts (**P5**, **P6**)—Scheme 1. The approach of reactants can proceed with the diastereofacial selectivity *anti* to *t*-BuO substituent or *syn* to it. Our previous experiments have shown that under the kinetic control a mixture of **P3** and **P5** can be formed in a ratio of about 5.7:1.[5] On the other hand, the mixture of **P3** and **P4** was obtained when the experiment was carried out in boiling toluene solution under thermodynamic conditions.[6] Moreover, in the latter case, the *exo*–*syn* adduct **P4** has been found to be the major one (**P4**:**P3** ratio 3:2). Such a result was unexpected, since to the best of our knowledge, the *exo*-approach in *syn* mode should be disfavored. The formation of this product has been reported by Brandi et al.,[16] but the authors did not provide details of the reaction conditions. Our careful studies and analysis, based on the NMR and CD spectra as well as on the rentgenostructural analysis, unambiguously confirmed the structure of compounds **P3**, **P4**, **P5** as well as the conditions of their formation.[5,6] The apparent stereochemical pathway of the reaction encouraged us to undertake a deeper analysis, involving computational methods.

Initially, the conformational studies for **P3**, **P4**, and **P5** adducts were performed. The same analysis was also carried out for the hypothetical adduct **P6**, which has not been observed.[5,6] In Figure 2, the two most stable conformers of each adduct are shown.

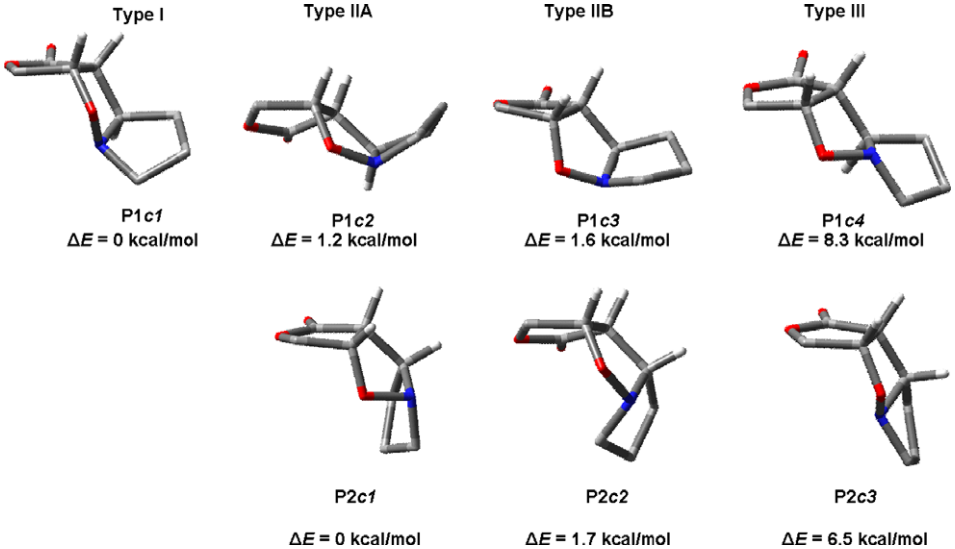


**Figure 1.** The conformers of adducts **P1** and **P2** with corresponding relative energies in kcal/mol (MM+ force field).

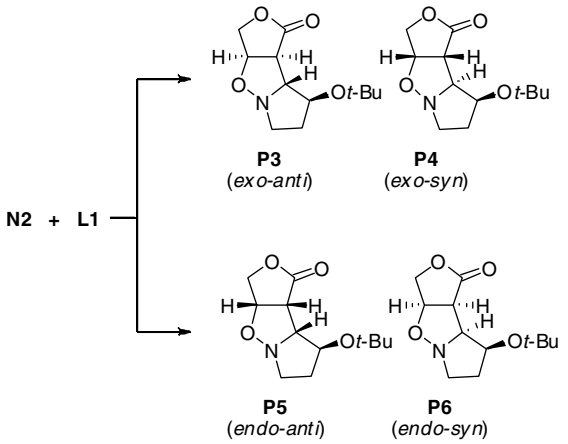


**Scheme 1.**

Similarly, as in the case of the **P1** cycloadduct, two sets of conformers (type I and II) were also found for **P3**, **P4**, and **P6**. Adduct **P5** behaves similarly as **P2** showing only type II conformers. For every type of conformer, several substructures were found resulting from the relative mobility of the *t*-BuO group. The energy differences between such substructures are small, and do not exceed 0.4 kcal/mol. Figure 3 presents the X-ray structures[17] for the cycloadducts **P3**, **P4**, and **P5**, and selected geometrical data are presented in Table 1.

The obtained results revealed that only a narrow range of $H_5$–$C_5$–O–*t*-Bu dihedral angles can be taken into consideration. The most favorable arrangement of the $H_5$ atom and *t*-Bu group is almost *syn*-periplanar with a small deviation of the corresponding dihedral angle in range of ±26° from 0° value (Scheme 2). Other conformations of the *t*-BuO group are strongly disfavored resulting from the apparent steric hindrance. For the **P3** adduct, the conformers with an *anti*-periplanar arrangement of $H_5$ atom and *t*-Bu group have ca. 7.5–9.0 kcal/mol higher energy than conformers with a lowest energy (Scheme 2). For other adducts, the corresponding energy difference is even larger. These distortions are well illustrated by the **P4** adduct in which the *t*-BuO group and isoxazolidine ring (fused to the lactone ring) are on the same side of the pyrrolidine moiety. The accurate values of the $H_5$–$C_5$–O–*t*-Bu dihedral angle for each adduct are presented in Table 1. The relative energies of these adducts are presented in Table 2. For each of the adducts, only the two lower energy conformers (both type) were taken into consideration.

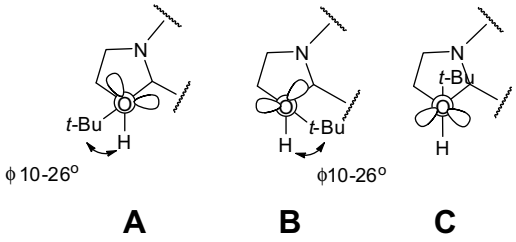


**Scheme 2.**

The main geometric parameters for all cycloadducts are collected in Table 1. In most cases, the lengths of $O_1$–$C_{1a}$, $C_{4a}$–$C_{4b}$, and $C_{4b}$–$N_8$ bonds are slightly shorter for the more stable ***c2*** conformers. An opposite trend is observed for the $C_{1a}$–$C_{4a}$ and $N_8$–$O_1$

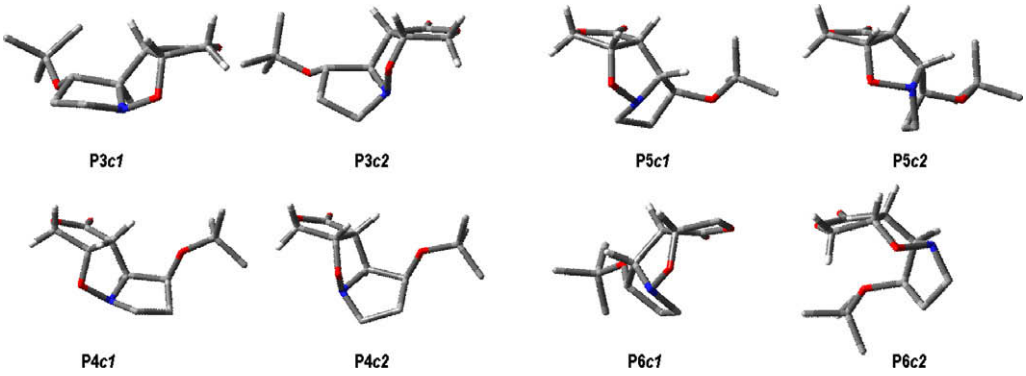


**Figure 2.** The conformers of adducts **P3**, **P4**, **P5** and **P6**.

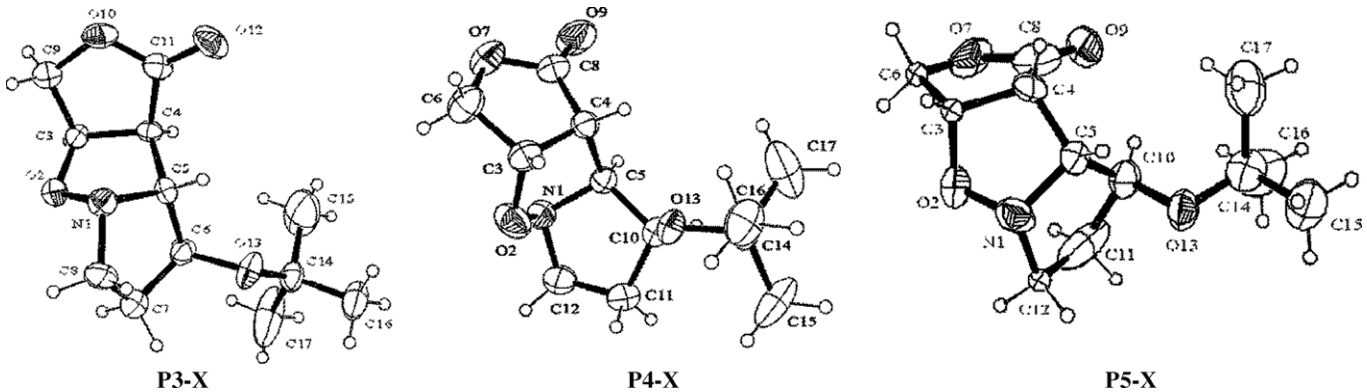


**Figure 3.** Molecular structures of the compounds **P3**–**X**, **P4**–**X** and **P5**–**X** with the crystallographic numbering scheme.[17]

**Table 1**
Several geometrical parameters of cycloadducts **P3**, **P4**, **P5** and **P6**

| | Bond lengths (Å) | | | | | Dihedral angles (°) | | | | |
|---|---|---|---|---|---|---|---|---|---|---|
| | $O_1$–$C_{1a}$ | $C_{1a}$–$C_{4a}$ | $C_{4a}$–$C_{4b}$ | $C_{4b}$–$N_8$ | $N_8$–$O_1$ | $\varphi_1$ | $\varphi_2$ | $\varphi_3$ | $\varphi_4$ | $\varphi_5$ |
| **P3*c1*** | 1.441 | 1.528 | 1.555 | 1.489 | 1.434 | 22.1 | −3.7 | 16.9 | 23.5 | 13.1 |
| **P3*c2*** | 1.419 | 1.544 | 1.539 | 1.481 | 1.487 | −6.1 | −22.9 | −4.5 | −1.2 | −23.3 |
| **P3–X** | 1.417 | 1.543 | 1.536 | 1.481 | 1.488 | −3.5 | −25.2 | −0.7 | 1.7 | −20.7 |
| **P4*c1*** | 1.442 | 1.526 | 1.545 | 1.496 | 1.435 | −23.1 | 5.8 | −18.0 | −23.1 | −15.9 |
| **P4*c2*** | 1.419 | 1.541 | 1.534 | 1.486 | 1.484 | 4.5 | 22.7 | 2.3 | 0.5 | −20.7 |
| **P4–X** | 1.418 | 1.538 | 1.529 | 1.484 | 1.486 | −0.1 | 26.4 | −3.4 | −4.2 | −21.6 |
| **P5*c1*** | 1.444 | 1.531 | 1.564 | 1.471 | 1.441 | −15.5 | 25.2 | −12.0 | −17.0 | 15.9 |
| **P5*c2*** | 1.416 | 1.536 | 1.554 | 1.506 | 1.478 | −26.0 | −2.7 | −17.0 | −26.0 | 14.9 |
| **P5–X** | 1.417 | 1.476 | 1.492 | 1.499 | 1.419 | −32.2 | 3.5 | −18.6 | −25.6 | 11.6 |
| **P6*c1*** | 1.451 | 1.532 | 1.555 | 1.462 | 1.448 | 25.2 | −34.6 | 18.1 | 24.8 | −27.3 |
| **P6*c2*** | 1.423 | 1.541 | 1.543 | 1.486 | 1.484 | −1.5 | −28.0 | 7.8 | 1.9 | 27.8 |

$\varphi_1$—the values of $O_1$–$C_{1a}$–$C_{4a}$–$C_{4b}$ dihedral angle.
$\varphi_2$—the values of $C_{1a}$–$C_{4a}$–$C_{4b}$–$N_8$ dihedral angle.
$\varphi_3$—the values of $C_4$–$C_{4b}$–$C_{4a}$–$C_2$ dihedral angle.
$\varphi_4$—the values of $H_{1a}$–$C_{1a}$–$C_{4a}$–$H_{4a}$ dihedral angle.
$\varphi_5$—the values of $H_5$–$C_5$–O–C($Me_3$) dihedral angle.
For atoms numbering see Scheme 1.

bonds; they are slightly longer for ***c2*** conformers. Only a single deviation from this trend was observed in the case of the $C_{4b}$–$N_8$ bond of *endo*-adducts, the length values of this bond are slightly larger for ***c2*** conformers than those for ***c1*** ones.

All cycloadditions are exothermic processes ranging from −11.9 to −20.5 kcal/mol. The energy difference ($\Delta\Delta H$) between both conformers of **P3** is ca. 1.4 kcal/mol. The corresponding values for **P4** and **P5** are ca. 0.8 and 2.1 kcal/mol, respectively. The calculations were also performed for the hypothetical adduct **P6**. In the latter case, the conformers' energy difference is ca. 4.2 kcal/mol.

Enthalpies and free energies of the adducts revealed that their stability increases successively in series **P6**, **P5**, **P3**, and **P4** (Table 1). The analysis of activation enthalpies for the TSs indicated that the *exo–anti* approach (**TS3**) is the most favorable one. The *endo–anti* (**TS5**) and the *exo–syn* (**TS4**) approaches have the activation barrier higher than **TS3** by ca. 0.9 and 2.0 kcal/mol, respectively. The hypothetical *endo–syn* approach (**TS6**) is strongly disfavored because of the steric interaction.

These results are in good agreement with our experimental studies.[5,6] Under the kinetic conditions, products with the lower activation energy should be obtained and indeed the cycloaddition affords a mixture of **P3** and **P5** adducts. The former one, having a lower activation energy, is the major product (Scheme 1). Also, the low temperature experiments (at −18 °C) demonstrated the lowest activation energy for **TS3**. Based on the free energy of activation for **TS3** and **TS5**, the approximate product ratio of 3.7:1 was assigned for the formation of **P3** and **P5**. The obtained value reflects the experimental products' ratio to be equal to about 5.7:1.[5]

Under thermodynamic control, the formation of **P3**/**P4** mixture was observed with predominance of the latter one.[6] The theoretical predictions for this process also correlate very well with the experimental results. The equilibrium ratio of **P3** and **P4**, based on their free energy values, is close to the experimental assignment (1:1.6 and 2:3, respectively). As was mentioned earlier, the higher stability of **P4** compared to **P3** was unexpected. To the best of our knowledge, the formation of *syn*-adducts is less favorable and indeed the activation energy of **TS4** supported this. The adduct **P4**, however, has an additional stabilizing effect which decreases its energy. The second order perturbation theory analysis of Fock matrix in NBO basis[18] shows the stabilizing effect between the lone pair of the oxygen atom of *t*-BuO group and the relatively acidic proton $H_{4a}$ located in α-position to the electron-withdrawing group ($n_O \rightarrow \sigma^*_{C-H}$, 0.6 kcal/mol, Fig. 4). Such an extra stabilization effect could account for **P4** to be thermodynamically more stable than **P3**. The interaction between $H_{4a}$ and the oxygen atom of *t*-BuO group is also established by NMR spectra. The signal of $H_{4a}$ proton is located downfield for **P4** in comparison to its position for **P3**, as well as for **P5**, which confirms an interaction between both atoms.[5,6]

**Table 2**
Relative energies: free energies ($\Delta G$, kcal/mol), enthalpies ($\Delta H$, kcal/mol), and entropies ($\Delta S$, cal/mol K) at 25 °C, for TSs and products of reaction between **N2** and **L1**[a]

| | Direct reaction | | | Inverse reaction | | |
|---|---|---|---|---|---|---|
| | $\Delta H$ | $\Delta S$ | $\Delta G$ | $\Delta H$ | $\Delta S$ | $\Delta G$ |
| **TS3** | 17.9 | −17.7 | 23.1 | 27.1 | 7.6 | 24.8 |
| **TS4** | 19.9 | −17.3 | 25.0 | 29.6 | 4.3 | 28.0 |
| **TS5** | 18.8 | −17.0 | 23.9 | 27.4 | 8.3 | 25.0 |
| **TS6** | 23.8 | −22.2 | 30.5 | 25.8 | 3.6 | 24.8 |
| **P3*c1*** | −18.8 | −49.5 | −4.1 | | | |
| **P3*c2*** | −20.2 | −47.5 | −6.1 | | | |
| **P4*c1*** | −19.7 | −49.1 | −5.1 | | | |
| **P4*c2*** | −20.5 | −47.6 | −6.3 | | | |
| **P5*c1*** | −17.3 | −48.0 | −3.0 | | | |
| **P5*c2*** | −19.4 | −48.8 | −4.9 | | | |
| **P6*c1*** | −11.9 | −48.3 | 2.5 | | | |
| **P6*c2*** | −16.1 | −52.3 | −0.5 | | | |

[a] All TS energies refer to the energy value of [N···L] van der Waals' molecular complex and energies of all adducts are referred to sum [N+L].

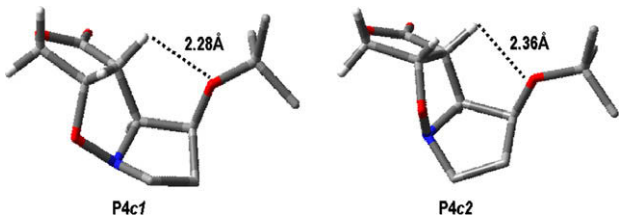


**Figure 4.** Extra stabilization of **P4** adduct by hydrogen bonding.

Several geometrical parameters for **TS3**, **TS4**, **TS5**, and **TS6** are collected in Table 3. In all cases, the $C_{1a}$–$O_1$ distance is shorter than $C_{4a}$–$C_{4b}$, which is typical for the cycloadditions with the electron-poor dipolarophiles.[8,21] Moreover, for both *exo* transition states the $C_{1a}$–$O_8$ distance is longer than that for *endo* TSs. The opposite trend was observed for the $C_{4a}$–$C_{4b}$ distance. For all TSs, the $O_1$–$C_{1a}$–$C_{4a}$–$C_{4b}$ dihedral angle value is close to zero, indicating that these four atoms are almost coplanar and only nitrogen atom is located out-of-plane. These results correlate very well with the

**Table 3**
Selected geometric parameters for transition structures **TS3**, **TS4**, **TS5**, and **TS6**

| | Bond lengths (Å) | | Dihedral angles | |
|---|---|---|---|---|
| | $C_{1a}$–$O_1$ | $C_{4a}$–$C_{4b}$ | $O_1$–$C_{1a}$–$C_{4a}$–$C_{4b}$ | $O_1$–$N_8$–$C_{4b}$–$C_{4a}$ |
| **TS3** | 1.909 | 2.230 | 6.9 | 49.3 |
| **TS4** | 1.935 | 2.200 | 2.2 | 47.2 |
| **TS5** | 1.861 | 2.500 | −0.4 | −43.3 |
| **TS6** | 1.871 | 2.222 | 7.5 | 46.8 |

For atoms numbering see Chart 2.

previous observation for **P1** and **P2**,[9] and show that the introduction of a *t*-BuO substituent to the nitrone molecule does not influence the geometry of the transition state significantly.

Previously, we have shown that adduct **P3** can be partially isomerized to adduct **P4** as a result of the increase of heating duration.[6] The same phenomenon was observed for **P5** which after prolonged heating gave the equilibrium mixture of **P4** and **P3**.[6] Figure 5 shows the changes of the adducts' ratio during isomerization of **P3**, and Figure 6 presents the changes of adducts' ratio during the heating of **P3**/**P5** mixture obtained under kinetic conditions. Both experiments reveal that the isomerization process is slow and that the equilibrium can usually be reached after 8 days with a significant decrease of overall yield, due to the low stability of nitrone.

The values of the energy barrier for the *retro*-1,3-cycloaddition reactions are shown in Table 2. For adducts, **P3**, **P4** and **P5**, the activation energy values of the reverse process are ca. 8.6–9.7 kcal/mol higher than for the synthesis, which indeed suggests that the *retro*-cycloaddition should be a slow process. The lowest value of activation energy of the reverse reaction was found for **P5** adduct, and the highest one was found for **P4** adduct. These results are in agreement with our experiments of isomerization of adducts discussed above.

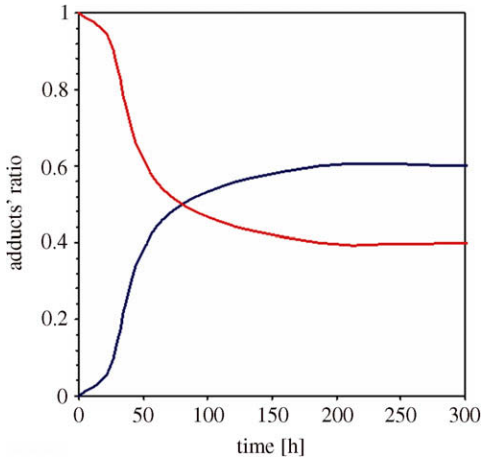


**Figure 5.** Changes of adducts' ratio during isomerization of adduct **P3** (—) to adduct **P4** (—).

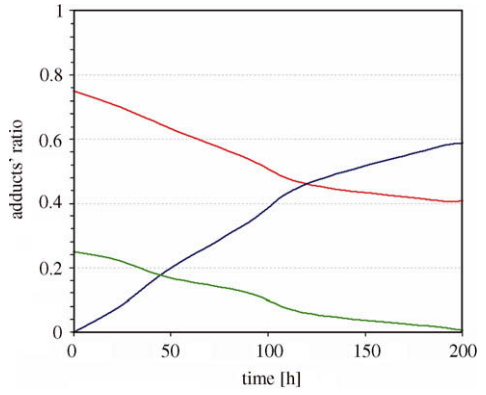


**Figure 6.** Changes of adducts' ratio during heating of **P3**/**P5** mixture obtained under kinetic control. Legend: **P3** (—), **P4** (—), and **P5** (—).

### 3.3. The 1,3-DC reaction of nitrone N1 and lactone L3—single asymmetric induction system

We focused our attention on the reaction of nitrone **N1** with the chiral lactone **L3**. The four possible products are depicted in Scheme 3. The hypothetical *endo*–*syn* adduct **P10** was omitted from further discussion for simplification.

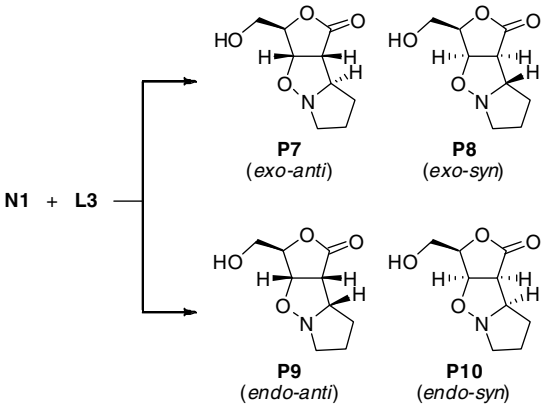


**Scheme 3.**

The result of conformational analysis of adducts **P7**, **P8**, and **P9** is analogous to previous examples. Only the discussion of rotation of the hydroxymethyl substituent is presented here.

For adducts **P7**, **P8**, and **P9** (both type I and II) there are three rotamers of the $CH_2OH$ group relative to the lactone moiety. These three conformations of this substituent are depicted in Scheme 4. The conformers **A** and **B** have similar energies, whereas the rotamer **C** is ca. 0.02–0.2 kcal/mol higher in energy than the former ones. The **C** conformation, however, was found to be particularly preferred in a solid state, resulting in a better fit within an elementary cell (see X-ray structures in Ref. 5).

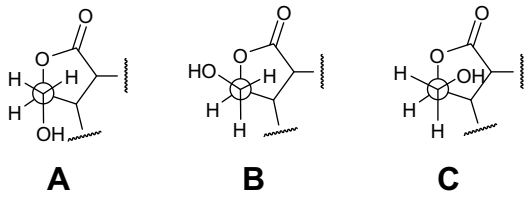


**Scheme 4.**

Analogously to the reaction of nitrone **N2** with **L1**, in the case of the **N1**–**L3** pair all possible directions of cycloaddition are exothermic processes in the range from −12.2 to −14.2 kcal/mol. The stability of the adducts increases in order **P9**, **P8** and **P7** (Table 4).

The calculated activation barriers reveal that the *exo*–*anti* approach is the most favorable (**TS7**). The *endo* approach (**TS9**) is ca. 0.6 kcal/mol ($\Delta\Delta H^{\ddagger}$) higher in energy. According to the computational results, the second *exo*-approach (*syn* addition to hydroxymethyl group of the lactone) is strongly disfavored. The activation enthalpy for **TS8** is ca. 7.8 kcal/mol higher than for the activation barrier of **TS7**.

**Table 4**
Relative energies: free energies (Δ*G*, kcal/mol), enthalpies (Δ*H*, kcal/mol), and entropies (Δ*S*, cal/mol K) at 25 °C, for TSs and products of reaction between **N1** and **L3**[a]

| | Direct reaction | | | Reverse reaction | | |
|---|---|---|---|---|---|---|
| | Δ*H* | Δ*S* | Δ*G* | Δ*H* | Δ*S* | Δ*G* |
| **TS7** | 17.2 | −19.9 | 23.1 | 27.8 | 2.0 | 27.2 |
| **TS8** | 25.0 | −11.5 | 28.5 | 28.8 | 2.2 | 28.1 |
| **TS9** | 17.8 | −18.5 | 23.3 | 26.2 | 0.7 | 26.0 |
| **P7*c1*** | −12.5 | −48.4 | 1.9 | | | |
| **P7*c2*** | −14.2 | −47.6 | 0.0 | | | |
| **P8*c1*** | −12.6 | −49.1 | 2.0 | | | |
| **P8*c2*** | −13.8 | −48.2 | 0.6 | | | |
| **P9*c1*** | −11.9 | −48.2 | 2.4 | | | |
| **P9*c2*** | −12.2 | −48.2 | 2.2 | | | |

[a] All TS energies refer to the energy value of [N···L] van der Waals' molecular complex and energies of all adducts are referred to sum [N+L].

The above results show that under kinetic control, the formation of **P7**/**P9** mixture should be expected. Moreover, such an expectation appeared justifiable when cycloaddition of nitrone **N1** to the lactone **L1** is taken into consideration.[7b,9] These predictions only partially agree with our experimental findings. According to our preliminary studies, cycloaddition of nitrone **N1** to lactone **L3** gave mixture of two adducts **P7** and **P8** in a ratio of about 7:3.[5] In case of minor product, we were unable to unambiguously establish its configuration by $^1$H NMR spectra. Moreover, rapid decomposition of **P8** was observed, which additionally complicated its analysis. Previously, we showed that CD spectroscopy is a convenient, sensitive, and rapid technique for the stereochemical assignment of products between nitrones **N1**, **N2** and six-membered lactones. These assignments are based on the 'ring-chirality rule' which correlates the positive/negative sign of the n–$\pi^*$ CD band (Cotton effect) with the positive/negative sign of the O–C(=O)–$C_\alpha$–$C_\beta$ torsional angle in lactone moiety.[19] Recently, we proved that the 'ring-chirality rule' can be applied also in case of the cycloaddition reaction involving five-membered lactones as well (**L1** and **L3**).[20] However, the assignment of **P8**'s configuration by CD spectra failed due to deviation from generally observed trends. One could suggest that partial isomerization of **P8** into more stable **P8′** may occur (Scheme 5). Such behavior, however, was not observed for the structurally related compound **P12**.

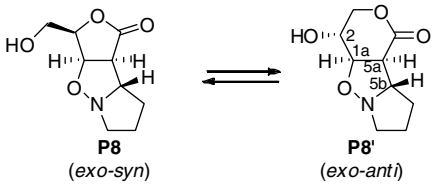


**Scheme 5.**

The discrepancy between the calculations and experiments forced us to carry out a deeper analysis of the investigated cycloaddition reaction. Its reinvestigation revealed the presence of *endo*-adduct **P9**. Due to its unexpected high polarity and a weak visualization on the TLC plates, it was lost in our preliminary experiments during the standard column chromatography. In repeated experiments, the mixture of adducts **P7**/**P8**/**P9** in a ratio ca. 78:7:15 was obtained. In a other experiment, where the silylated lactone (protected with TBDPS) was used instead of the unprotected lactone **L3**, the mixture of silylated cycloadducts **P7** and **P9** (**Si**–**P7**, **Si**–**P9**) was obtained in the ratio 94:6, exclusively. The silylated derivative of **P8** was not observed. Hence, after the above revision, the theoretical predictions about cycloaddition of nitrone **N1** to lactone **L3** fit well with the experimental findings.

### 3.4. The 1,3-DC reaction of nitrone N2 and lactone L3—double asymmetric induction system

The 1,3-DC reaction of nitrone **N2** to chiral lactone **L3** is shown in Scheme 6. According to our previous studies, the three adducts **P11**, **P12** and **P13** are formed in a ratio ca. 21:27:52. The formation of the *endo–syn* **P14** cycloadduct has never been observed, and therefore it was omitted from further analysis. The preference for the *endo* product **P13** formation is attributable to the mismatched effect of substituents at both reactants in the *exo*-approach.

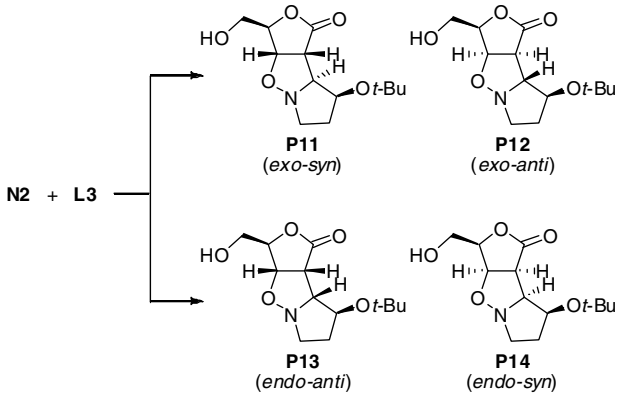


**Scheme 6.**

Due to the influence of the three independent factors on the conformational properties (tricyclic fused system, *t*-BuO group in the pyrrolidine ring, and hydroxymethyl group in the lactone), the conformational analysis of the cycloaddition reaction between the nitrone **N2** and the lactone **L3** is more complicated than that for the single asymmetric induction case (see Sections 3.1–3.3). The general trends, however, found in previous cases, are still observed. For adducts **P11** and **P12**, the most stable type I conformer and two separate type II conformers were found. Analogously, as it was observed that in the case of the adducts **P2**, **P5**, and **P9**, only the type II conformers were found for the adduct **P13**. For each type of the tricyclic fused system, several substructures were found due to the different arrangement of both substituents. The calculations predicted the preference of the *anti*-periplanar arrangement of the OH group and the lactones' oxygen atom (conformer A, Scheme 4) and similar in energy *gauche* conformation B. The *t*-BuO group and the $H_5$ atom are in a *syn*-periplanar conformation. The more complex character of conformational interactions makes the energy differences between particular types of conformers larger than those found in previous cases. Although for the **P11** ***c2*–*c1***, the enthalpy difference is only 1.8 kcal/mol, the corresponding values for two other products **P12** and **P13** are higher and amount to 5.5 and 10.5 kcal/mol (Table 5).

**Table 5**
Relative energies: free energies (Δ*G*, kcal/mol), enthalpies (Δ*H*, kcal/mol), and entropies (Δ*S*, cal/mol K) at 25 °C, for TSs and products of reaction between **N2** and **L3**[a]

| | Direct reaction | | | Reverse reaction | | |
|---|---|---|---|---|---|---|
| | Δ*H* | Δ*S* | Δ*G* | Δ*H* | Δ*S* | Δ*G* |
| **TS11** | 19.1 | −16.8 | 24.1 | 28.4 | 2.5 | 27.6 |
| **TS12** | 19.1 | −17.5 | 24.3 | 25.1 | 4.2 | 23.9 |
| **TS13** | 18.7 | −19.4 | 24.5 | 23.8 | 1.8 | 23.3 |
| **P11*c1*** | −19.3 | −48.5 | −4.8 | | | |
| **P11*c2*** | −21.1 | −47.5 | −6.9 | | | |
| **P12*c1*** | −14.2 | −48.2 | 0.1 | | | |
| **P12*c2*** | −19.7 | −47.4 | −5.6 | | | |
| **P13*c1*** | −8.6 | −49.8 | 6.2 | | | |
| **P13*c2*** | −19.4 | −48.9 | −4.9 | | | |

[a] All TS energies refer to the energy value of [N···L] van der Waals' molecular complex and energies of all adducts are referred to sum [N+L].

The geometry optimization of adducts revealed that the *syn*-adduct **P11** is ca. 1.4 kcal/mol lower in energy than the *anti*-adduct **P12** (Table 5), analogously to the **P3**/**P4** pair (Table 2). On the other hand, the **P12** and **P13** have an analogous stability, and the energy difference between them is only 0.3 kcal/mol which is smaller than that for the **P3**/**P5** pair, which was found to be 0.8 kcal/mol.

The activation enthalpy values confirm the experimental observations that the *endo*-adduct is a kinetic product of the reaction (Table 5). The activation barrier for both *exo*-adducts is the same, and is ca. 0.4 kcal/mol higher than that for **TS13**. On the other hand, the activation enthalpies for the reverse reaction are higher and fall within the range of 5.1–9.3 kcal/mol (Table 5). The *retro*-process is the easiest for adduct **P13**, and is more difficult for adduct **P11**.

As we pointed out,[5,6] the reversibility of this cycloaddition is not straightforward. The long heating time of the reaction mixture leads to the slow disappearance of the *endo*-adduct **P13**. It does not lead, however, to the most stable **P11** adduct or **P11**/**P12** mixture as observed for the **P3**/**P4** pair. In this case, the formation of adduct **P15** (Scheme 7) arises because of the thermal racemization of the lactone via a hydroxyfuran stage, as well as of the slow decomposition of the nitrone being observed, hence the thermodynamic equilibrium cannot be reached.

The increase in the amount of **P15** in the reaction mixture is attributable to its very low activation enthalpy (**TS15**, Table 6). This value is ca. 4.5 kcal/mol lower than that for **TS13**. Moreover, the barrier for the *retro*-process is almost twice as high than that for the synthesis which makes the reversibility of this process difficult. Additionally, the lower **TS15** energy value upsets the **L3**/*ent*-**L3** equilibrium by consuming the *ent*-**L3**. These factors appear to contribute to the experimental observation that the **P15** adduct is the major product of the reaction under thermodynamic conditions.

Generally, the cycloaddition of nitrone **N2** to *ent*-**L3** can afford up to four cycloadducts as presented in Scheme 7. Owing to the matching of the reactants, however, the cycloaddition proceeds with a high diastereoselectivity and leads to the *exo–anti* adduct **P15** exclusively.

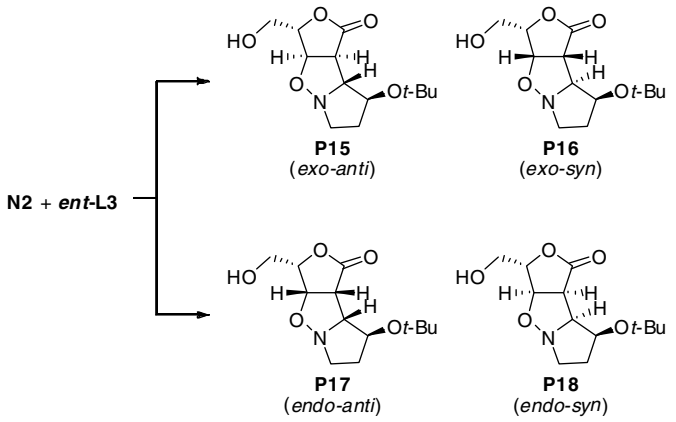


**Scheme 7.**

The activation enthalpy for adduct **P15** (**TS15**) is only 14.2 kcal/mol, and is much lower than that for other adducts, hence, it explains the high stereoselectivity of the cycloaddition (Table 6).

The computational predictions correspond very well with the experimental findings. Moreover, they explain some other observations. For example, when the cycloaddition of **N1** to **L3** was carried out in triethylamine in the presence of trace amounts of water, the mixture of adducts **P15** and **P13** was obtained in a 4:1 ratio.

Under these reaction conditions, the base-mediated racemization of **L3** occurs faster and we hoped that the dynamic kinetic resolution of the lactone can be achieved. This approach would be an attractive way for the synthesis of adducts derived from the *ent*-**L3**, predominantly due to its relative poor availability compared to the commercially available (*S*)-enantiomer.

**Table 6**
Relative energies: free energies ($\Delta G$, kcal/mol), enthalpies ($\Delta H$, kcal/mol), and entropies ($\Delta S$, cal/mol K) at 25 °C, for TSs and products of reaction between **N2** and ***ent*-L3**[a]

| | Direct reaction | | | Reverse reaction | | |
|---|---|---|---|---|---|---|
| | $\Delta H$ | $\Delta S$ | $\Delta G$ | $\Delta H$ | $\Delta S$ | $\Delta G$ |
| **TS15** | 14.2 | −10.8 | 17.5 | 27.4 | 2.4 | 26.7 |
| **TS16** | 28.2 | −12.8 | 32.0 | 29.8 | 3.1 | 28.8 |
| **TS17** | 28.1 | −14.0 | 32.2 | 26.1 | −1.5 | 26.5 |
| **TS18** | 30.0 | −17.2 | 35.1 | 27.7 | 5.8 | 25.9 |
| **P15*c1*** | −15.3 | −47.0 | −1.3 | | | |
| **P15*c2*** | −20.3 | −47.6 | −6.1 | | | |
| **P16*c1*** | −16.8 | −48.3 | −2.4 | | | |
| **P16*c2*** | −16.4 | −47.9 | −2.2 | | | |
| **P17*c1*** | −14.6 | −45.2 | −1.1 | | | |
| **P17*c2*** | −14.2 | −47.4 | −0.1 | | | |
| **P18*c1*** | −12.1 | −47.5 | 2.0 | | | |
| **P18*c2*** | −13.7 | −50.6 | 1.4 | | | |

[a] All TS energies refer to the energy value of [N···L] van der Waals' molecular complex and energies of all adducts are referred to sum [N+L].

According to the computational predictions, the difference of activation enthalpy between **TS15** and **TS13** is ca. 4.5 kcal/mol, which indicates that the adduct **P15** should be formed exclusively. The experimentally obtained **P15**/**P13** ratio (4:1) does not agree with the predictions. Due to arguments presented above, however, we are unable to prove that the thermodynamic equilibrium has been reached.

## 4. Conclusions

The presented study demonstrates that the DFT calculations at B3LYP/6-31+G(d) level of theory can be used for the detailed description of the cycloaddition reaction between the five-membered cyclic nitrones and five-membered lactones. The above methodology is applicable, not only to the simplest model systems such as **N1**/**L2** providing simple tricyclic fused ring systems, but also to the analysis of cycloadditions involving substituted reactants. The quantum-mechanic calculations in combination with the molecular modeling are in the agreement with the experimentally observed trends in the 1,3-dipolar cycloaddition reactions of nitrones **N1** and **N2** with unsaturated γ-lactones. Computational predictions successfully reproduced the *exo*/*endo* selectivity as well as the diastereofacial selectivity connected with the inductive effect of substituents.[5,6] As was pointed out for the cycloaddition of **N1** to lactone **L3**, the computational methods in combination with the spectroscopy data can be a most useful analytical tool for the study of organic reactions, and can provide help in resolving some stereochemical controversies.

## 5. Experimental

Proton and carbon NMR spectra were recorded on a Bruker DRX 500 Avance Spectrometer at 500 MHz and 125 MHz, respectively, using deuterated solvents and TMS as an internal standard. Chemical shifts are reported as $\delta$ values in ppm and coupling constants are in hertz. Infrared spectra were recorded on an FT-IR-1600 Perkin–Elmer spectrophotometer. The optical rotations were measured with a JASCO J-2000 digital polarimeter. High resolution mass spectra were recorded on ESI-TOF Mariner spectrometer (Perspective Biosystem). The HPLC analysis was carried out on Hitachi chromatograph with L-2130 pump and L-2450 DAD detector equipped with LiChrospher® Si60 analytical column.

Thin layer chromatography (TLC) was performed on aluminum sheets Silica Gel 60 $F_{254}$ (20 × 20 × 0.2) from Merck. Column chromatography was carried out using Merck silica gel 230–400 mesh. The TLC spots were visualized in UV (254 nm) and by treatment with alcoholic solution of ninhydrine, aqueous solution of $KMnO_4$, or with ceric sulphate/phosphomolybdenic acid solution.

Toluene was purified and dried by applying standard techniques.[22] The TBDPS protected lactone **L3** (**Si–L3**) was prepared according to literature procedure from commercially available lactone **L3** (Fluka).[23] Nitrone **N1** was obtained from 1,4-dibromobutane.[24]

### 5.1. Isomerization of P3

A sample of **P3** (75 mg)[5] in dry toluene (10 mL) was refluxed under an argon atmosphere. The progress of isomerization was monitored by TLC, and the **P3**/**P4** ratio was assigned by $^1$H NMR spectra in benzene-$d_6$. After ca. 8 days, equilibrium mixture was obtained (**P4**/**P3** ratio 3:2). For spectral data of **P3** and **P4**, see Refs. 5 and 6, respectively.

### 5.2. Cycloaddition of nitrone N1 to lactone L3

The lactone **L3** (100 mg, 0.88 mmol) and nitrone **N1** (96 mg, 1.14 mmol) were dissolved in dry toluene (10 mL) and stirred at room temperature under an argon atmosphere. The progress of reaction was monitored by TLC (ethyl acetate–hexane 4:1). After disappearance of the lactone, the solvent was removed and the residue was chromatographed on silica gel (ethyl acetate–hexane 2:1 with the addition of 1% triethylamine) affording adducts **P7** (95 mg) and **P8** (8 mg). The adduct **P9** was eluted with ethyl acetate (18 mg). Overall yield was 70%. For analytical data of **P7** and **P8**, see Ref. 5.

### 5.3. (1*aS*,2*R*,4*aR*,4*bS*)-2-Hydroxymethyl-hexahydrofuro-[3,4-*d*]pyrrolo[1,2-*b*]isoxazol-4(3*H*)-one P9

Colorless oil; $[\alpha]_D = -67.4$ (*c* 0.6, $CH_2Cl_2$); $^1$H NMR (500 MHz, $C_6D_6$ with 5% $CD_3OD$): $\delta$ 4.60 (1H, d, *J* 6.3 Hz, H-1a), 4.19 (1H, dd, *J* 2.7, 2.2 Hz, H-2), 3.59 (1H, dd, *J* 9.6, 6.3 Hz, H-4a), 3.54–3.48 (2H, m, CH*H*OH, H-4b), 3.26 (1H, dd, *J* 12.3, 2.2 Hz, C*H*HOH), 3.12 (1H, ddd, *J* 13.6, 7.3, 4.1 Hz, H-7), 2.55 (1H, ddd, *J* 13.6, 8.3, 7.8 Hz, H-7′), 2.08–2.00 (1H, m, H-5), 1.75–1.64 (1H, m, H-6), 1.56–1.47 (1H, m, H-5′), 1.30–1.22 (1H, m, H-6′); $^{13}$C NMR (125 MHz, $C_6D_6$ with 5% $CD_3OD$): $\delta$ 176.2, 82.1, 81.8, 68.3, 62.1, 55.8, 53.7, 26.6, 24.5; IR (film, $CH_2Cl_2$) *v*: 3360, 1767 cm$^{-1}$; HR MS (ESI): *m/z* [M+H$^+$], calcd for $C_9H_{14}NO_4$ 200.0917. Found 200.0921.

### 5.4. Cycloaddition of nitrone N1 to Si–L3

The lactone **Si–L3** (154 mg, 0.44 mmol) and nitrone **N1** (48 mg, 0.57 mmol) were dissolved in dry toluene (10 mL) and stirred at room temperature under an argon atmosphere. The progress of the reaction was monitored by TLC (ethyl acetate–hexane 1:4). After disappearance of the lactone, the solvent was removed and the residue was chromatographed on silica gel (hexane–ethyl acetate 4:1) to afford adducts **Si–P7** and **Si–P9** in a 94:6 ratio (HPLC, hexane–2-propanol 97:3, 1 mL/min, $t_{Si-P7}$ 4.7 min, $t_{Si-P9}$ 10.3 min) with an overall yield of 73%.

### 5.5. (1*aS*,2R,4*aR*,4*bR*)-2-(*tert*-Butyldiphenylsilyloxymethyl)-hexahydrofuro[3,4-*d*]pyrrolo[1,2-*b*]isoxazol-4(3*H*)-one Si–P7

Colorless oil; $[\alpha]_D = +37.5$ (*c* 1.2, $CH_2Cl_2$); $^1$H NMR (500 MHz, $C_6D_6$): $\delta$ 7.80–7.18 (10H, 2 × Ph), 4.60 (1H, d, *J* 7.2 Hz, H-1a), 4.43 (1 H, dd, *J* 2.8, 2.3 Hz, H-2), 3.69 (1H, m, H-4b), 3.58 (1H, dd, *J* 11.4, 2.8 Hz, C*H*HOSi), 3.32–3.28 (2H, m, *J* 11.4, 7.2, 2.3 Hz, H-4a, CH*H*OSi), 3.22 (1H, ddd, *J* 14.0, 8.0, 3.3 Hz, H-7), 2.66 (1H, m, H-7′), 1.73 (1H, m, H-6), 1.45 (1H, m, H-5), 1.27–1.15 (2H, m, H-5′, H-6′), 1.10 (9H, s, *t*-Bu); $^{13}$C NMR (125 MHz, $C_6D_6$): $\delta$ 175.8, 136.0, 135.8, 133.3, 132.6, 130.3, 130.2, 128.5, 128.3, 85.3, 78.8, 70.9, 64.4, 56.04, 55.98, 30.0, 26.9, 24.4, 19.3; IR (film, $CH_2Cl_2$) *v*: 1769 cm$^{-1}$; HR MS (ESI): *m/z* [M+Na$^+$], calcd for $C_{25}H_{31}NO_4NaSi$ 460.1914. Found 460.1892.

### 5.6. (1*aS*,2*R*,4*aR*,4*bS*)-2-(*tert*-Butyldiphenylsilyloxymethyl)-hexahydrofuro[3,4-*d*]pyrrolo[1,2-*b*]isoxazol-4(3*H*)-one (Si–P9)

Colorless oil; $[\alpha]_D = -37.7$ (*c* 1.06, $CH_2Cl_2$); $^1$H NMR (500 MHz, $C_6D_6$ with 5% $CD_3OD$): $\delta$ 7.70–7.18 (10H, 2 × Ph), 4.66 (1H, d, *J* 6.4 Hz, H-1a), 4.14 (1H, dd, *J* 2.6, 1.9 Hz, H-2), 4.02 (1H, m, H-4b), 3.73 (1H, d, *J* 9.5, 6.4 Hz, H-4a), 3.53 (1H, dd, *J* 11.6, 2.6 Hz, C*H*HO-Si), 3.21 (1H, dd, *J* 11.6, 1.9 Hz, CH*H*OSi), 3.17 (1H, ddd, *J* 13.7, 7.5, 4.2 Hz, H-7), 2.61(1H, m, H-7′), 2.05 (1H, m, H-5), 1.75 (1H, m, H-6), 1.58 (1H, m, H-5′), 1.32 (1H, m, H-6′), 1.05 (9H, s, *t*-Bu); $^{13}$C NMR (125 MHz, $C_6D_6$ with 5% $CD_3OD$): $\delta$ 175.6, 135.9, 135.8, 132.9, 132.3, 130.4, 130.3, 128.5, 128.3, 81.7, 81.5, 68.2, 64.3, 55.7, 55.2, 26.8, 26.7, 24.6, 19.2; IR (film, $CH_2Cl_2$) *v*: 1771 cm$^{-1}$; HR MS (ESI): *m/z* [M+Na$^+$], calcd for $C_{25}H_{31}NO_4NaSi$ 460.1914. Found 460.1909.

## Acknowledgments

Authors are most indebted to the Department de Chimie Moleculaire (UJF, Grenoble), CIMENT/CECIC (Grenoble), and CERMAV (CNRS, Grenoble) and to Mr. Grzegorz Lipner (IOC PAS, Warsaw) for providing us with computer capabilities. We are also indebted to Marie Curie European Program for financial support for one of us (S.S.). Financial support for this work was provided through the Polish Ministry of Science and Informatics (Grant # 3 T09A 025 28).

## References

1. (a) Padwa, A. *1,3-Dipolar Cycloaddition Chemistry*; Wiley: New York, 1984; (b) Gothelf, K. V.; Jørgensen, K. A. *Chem. Rev.* **1998**, *98*, 863–909; (c) Karlsson, S.; Högberg, H.-E. *Org. Prep. Proced. Int.* **2001**, *33*, 103–172; (d) Kobayashi, S.; Jørgensen, K. A. *Cycloaddition Reactions in Organic Synthesis*; Wiley-VCH: Weinheim, 2002; (e) Pellissier, H. *Tetrahedron* **2007**, *63*, 3235–3285; (f) Padwa, A. *Synthetic Applications of 1,3-Dipolar Cycloaddition Chemistry Toward Heterocycles and Natural Products*; Padwa, A., Pearson, W. H., Eds.; Wiley & Sons: Hoboken, NJ, 2003; (g) Merino, P. *Science of Synthesis*; Padwa, A., Ed.; George Thieme: New York, NY, 2004, Vol. 27, p 511.
2. Frederickson, M. *Tetrahedron* **1997**, *53*, 403–425.
3. (a) Socha, D.; Jurczak, M.; Chmielewski, M. *Carbohydr. Res.* **2001**, *336*, 315–318; (b) Socha, D.; Paśniczek, K.; Jurczak, M.; Solecka, J.; Chmielewski, M. *Carbohydr. Res.* **2006**, *341*, 2005–2011; (c) Paśniczek, K.; Socha, D.; Solecka, J.; Jurczak, M.; Chmielewski, M. *Can. J. Chem.* **2006**, *84*, 534–539; (d) Panfil, I.; Solecka, J.; Chmielewski, M. *J. Carbohydr. Chem.* **2006**, *25*, 673–684; (e) Paśniczek, K.; Solecka, J.; Chmielewski, M. *J. Carbohydr. Chem.* **2007**, *26*, 195–211; (f) Stecko, S.; Jurczak, M.; Urbańczyk-Lipkowska, Z.; Chmielewski, M. *Carbohydr. Res.* **2008**, *343*, 2215–2220.
4. (a) Paśniczek, K.; Socha, D.; Jurczak, M.; Frelek, J.; Suszczyńska, A.; Urbańczyk-Lipkowska, Z.; Chmielewski, M. *J. Carbohydr. Chem.* **2003**, *22*, 613–629; (b) Socha, D.; Jurczak, M.; Frelek, J.; Klimek, A.; Rabiczko, J.; Urbańczyk-Lipkowska, Z.; Suwińska, K.; Chmielewski, M.; Cardona, F.; Goti, A.; Brandi, A. *Tetrahedron: Asymmetry* **2001**, *12*, 3163–3172; (c) Jurczak, M.; Rabiczko, J.; Socha, D.; Chmielewski, M.; Cardona, F.; Goti, A.; Brandi, A. *Tetrahedron: Asymmetry* **2000**, *11*, 2015–2022.
5. Stecko, S.; Paśniczek, K.; Jurczak, M.; Urbańczyk-Lipkowska, Z.; Chmielewski, M. *Tetrahedron: Asymmetry* **2006**, *17*, 68–79.
6. Stecko, S.; Paśniczek, K.; Jurczak, M.; Urbańczyk-Lipkowska, Z.; Chmielewski, M. *Tetrahedron: Asymmetry* **2007**, *18*, 1085–1093.
7. (a) Cid, P.; de March, P.; Figueredo, M.; Font, J.; Milan, S. *Tetrahedron Lett.* **1992**, *33*, 667–670; (b) Alonso-Perarnau, D.; de March, P.; Figueredo, M.; Font, J.; Soria, A. *Tetrahedron* **1993**, *49*, 4267–4274; (c) Cid, P.; de March, P.; Figueredo, M.; Font, J.; Milan, S.; Soria, A.; Virgili, A. *Tetrahedron* **1993**, *49*, 3857–3870.
8. Stecko, S.; Paśniczek, K.; Michel, C.; Milet, A.; Perez, S.; Chmielewski, M. *Tetrahedron: Asymmetry* **2008**. doi:10.1016/j.tetasy.2008.07.008.
9. Tufariello, J.; Tette, J. *J. Org. Chem.* **1975**, *40*, 3866–3869.

10. Kakisawa, H.; Iwashita, T.; Kusumi, T. *J. Org. Chem.* **1982**, *47*, 230–233.
11. Frisch, M. J.; Trucks, G. W.; Schlegel, H. B.; Scuseria, G. E.; Robb, M. A.; Cheeseman, J. R.; Montgomery, Jr., J. A.; Vreven, T.; Kudin, K. N.; Burant, J. C.; Millam, J. M.; Iyengar, S. S.; Tomasi, J.; Barone, V.; Mennucci, B.; Cossi, M.; Scalmani, G.; Rega, N.; Petersson, G. A.; Nakatsuji, H.; Hada, M.; Ehara, M.; Toyota, K.; Fukuda, R.; Hasegawa, J.; Ishida, M.; Nakajima, T.; Honda, Y.; Kitao, O.; Nakai, H.; Klene, M.; Li, X.; Knox, J. E.; Hratchian, H. P.; Cross, J. B.; Bakken, V.; Adamo, C.; Jaramillo, J.; Gomperts, R.; Stratmann, R. E.; Yazyev, O.; Austin, A. J.; Cammi, R.; Pomelli, C.; Ochterski, J. W.; Ayala, P. Y.; Morokuma, K.; Voth, G. A.; Salvador, P.; Dannenberg, J. J.; Zakrzewski, V. G.; Dapprich, S.; Daniels, A. D.; Strain, M. C.; Farkas, O.; Malick, D. K.; Rabuck, A. D.; Raghavachari, K.; Foresman, J. B.; Ortiz, J. V.; Cui, Q.; Baboul, A. G.; Clifford, S.; Cioslowski, J.; Stefanov, B. B.; Liu, G.; Liashenko, A.; Piskorz, P.; Komaromi, I.; Martin, R. L.; Fox, D. J.; Keith, T.; Al-Laham, M. A.; Peng, C. Y.; Nanayakkara, A.; Challacombe, M.; Gill, P. M. W.; Johnson, B.; Chen, W.; Wong, M. W.; Gonzalez, C.; Pople, J. A. GAUSSIAN *03, Revision B.04*; Gaussian: Pittsburgh, PA, 2003.
12. (a) Becke, A. D. *J. Chem. Phys.* **1993**, *98*, 5648–5652; (b) Becke, A. D. *Phys. Rev. A* **1988**, *38*, 3098–3100; (c) Lee, C.; Yang, W.; Parr, R. G. *Phys. Rev. B* **1988**, *37*, 785–789.
13. Schlegel, H. B. Geometry Optimization on Potential Energy Surface. In *Modern Electronic Structure Theory*; Yarkony, D. R., Ed.; World Scientific Publishing: Singapore, 1994.
14. Reed, A. E.; Weinstock, R. B.; Weinhold, F. *J. Chem. Phys.* **1985**, *83*, 735–746.
15. (a) Fukui, K. *Acc. Chem. Res.* **1981**, *14*, 363–368; (b) Head-Gordon, M.; Pople, J. A. *J. Chem. Phys.* **1988**, *89*, 5777–5786.
16. Goti, A.; Cicchi, S.; Cordero, F. M.; Fedi, V.; Brandi, A. *Molecules* **1999**, *4*, 1–12.
17. Crystallographic data for the structures reported in this paper have been previously deposited with the Cambridge Crystallographic Data Center, Cambridge, UK, as a Supplementary publications: **P3**–**X** (CCDC 282892), **P4**–**X** (CCDC 634391), and **P5**–**X** (CCDC 634282).
18. Weinhold, F.. In *Encyclopedia of Computational Chemistry*; Schleyer, P., Allinger, N. L., Clark, T., Gasteiger, J., Kollman, P. A., Schaefer, H. F., Eds.; Wiley: Chichester, UK, 1998; Vol. 3, pp 1792–1811.
19. Legrand, M.; Bucourt, R. *Bull. Soc. Chim. Fr.* **1967**, 2241–2242.
20. Stecko, S., Frelek, J., Chmielewski, M., in preparation.
21. (a) Carda, M.; Portoles, P.; Murga, J.; Uriel, S.; Marco, J. A.; Domingo, L. R.; Zaragoza, R.; Röper, H. *J. Org. Chem.* **2000**, *65*, 7000–7009; (b) Merino, P.; Mates, J. A.; Revuelta, J.; Tejero, T.; Chiacchio, U.; Romeo, G.; Iannazze, D.; Romeo, R. *Tetrahedron: Asymmetry* **2002**, *13*, 173–190; (c) Merino, P.; Revualta, J.; Tejero, T.; Chiacchio, U.; Rescifina, A.; Romeo, G. *Tetrahedron* **2003**, *59*, 3581–3592; (d) Merino, P.; Tejero, T.; Chiaccio, U.; Romeo, G.; Rescifina, A. *Tetrahedron* **2007**, *63*, 1448–1458.
22. Armarego, W.; Chai, C. *Purification of Laboratory Chemicals*, 5th ed.; Butterworth-Heinemann, 2003.
23. Mann, J.; Weymouth-Wilson, A. *Org. Synth.* **1998**, *75*, 139–142.
24. Cordero, F.; Machetti, F.; de Sarlo, F.; Brandi, A. *Gazz. Chim. Ital.* **1997**, *127*, 25–29.